Manifesting the evolution of eigenstates from quantum billiards to singular billiards in the strongly coupled limit with a truncated basis by using *RLC* networks

P. H. Tuan,[1] H. C. Liang,[2] J. C. Tung,[1] P. Y. Chiang,[1] K. F. Huang,[1] and Y. F. Chen[1,*]

[1]*Department of Electrophysics, National Chiao Tung University, 1001 Ta-Hsueh Road, Hsinchu 30010, Taiwan*

[2]*Institute of Optoelectronic Science, National Taiwan Ocean University, 2 Pei-Ning Road, Keelung 20224, Taiwan*

(Received 27 June 2015; revised manuscript received 28 October 2015; published 7 December 2015)

The coupling interaction between the driving source and the *RLC* network is explored and characterized as the effective impedance. The mathematical form of the derived effective impedance is verified to be identical to the meromorphic function of the singular billiards with a truncated basis. By using the derived impedance function, the resonant modes of the *RLC* network can be divided into the open-circuit and short-circuit states to manifest the evolution of eigenvalues and eigenstates from closed quantum billiards to the singular billiards with a truncated basis in the strongly coupled limit. The substantial differences of the wave patterns between the uncoupled and strongly coupled eigenmodes in the two-dimensional wave systems can be clearly revealed with the *RLC* network. Finally, the short-circuit resonant states are exploited to confirm that the experimental Chladni nodal-line patterns in the vibrating plate are the resonant modes subject to the strong coupling between the oscillation system and the driving source.

DOI: 10.1103/PhysRevE.92.062906 PACS number(s): 05.45.Mt, 73.63.Kv, 84.30.−r

I. INTRODUCTION

The interaction between the resonator and an exciter or a scatterer is commonly divided into a weak- and a strong-coupling regime. Starting with Šeba [1], quantum billiards with a point scatterer have been employed extensively to explore the coupling strength on the transition between integrable and chaotic features in quantum systems [2–8]. An analogous phenomenon in acoustics, the coupling of the string vibrations to the resonant modes of the supporting cavity, leads to a set of normal modes that can also be classified as weakly or strongly coupled depending on the coupling strength and the amount of damping [9]. Similarly, in cavity quantum electrodynamics the eigenmodes of the coupled dipole-cavity system are no longer original cavity modes but mixed light-dipole modes when the perturbative weak-coupling regime breaks and instead strong coupling takes place [10].

A simple damped harmonic oscillator is known to be physically equivalent to a single *RLC* circuit. Two coupled harmonic oscillators are a popular model for many physical systems, including atoms in external fields [11], coupled quantum dots [12], cavity optomechanics [13], and the stringed musical instruments [9]. As a result, the two-dimensional (2D) *RLC* circuit network is expected to be a promising model to reveal the coupling interaction between the 2D wave system and an exciter or a scatterer. With the isomorphism between the Kirchhoff's node equation and the discretized Helmholtz equation, Bulgakov *et al.* [14] and Bengtsson *et al.* [15] have employed the *RLC* circuit network to emulate the eigenmodes of quantum billiards with arbitrary shapes by varying the grounded grids of electrical circuits. Even though the *RLC* circuit network is intrinsically a driven oscillating system instead of a source-free system, the network model has not been developed to explore the variation of resonant modes with the coupling interaction of the driving source.

In this work, an analytical formula for the effective impedance $Z_{\text{eff}}(x_s, y_s; \omega)$ is derived as a function of the driving frequency ω and the source location (x_s, y_s) to characterize the coupling interaction between the driving source and the *RLC* network. The mathematical form of the effective impedance $Z_{\text{eff}}(x_s, y_s; \omega)$ is explicitly identical to the meromorphic function of the singular billiard with a truncated basis [3]. This sameness confirms that the *RLC* circuit network can be exploited to manifest the eigenvalues and eigenfunctions of the quantum billiards interacting with the inside scatterer in the weak- and strong-coupling regimes. With the derived impedance function, the resonant modes of the *RLC* network can be divided into the open-circuit and short-circuit states. The resonant spectrum of the short-circuit states exactly mimic the eigenvalues of the singular billiard with a truncated basis in the strong-coupling regime, whereas the resonant spectrum of the open-circuit states generally manifest the eigenvalues of the free billiards. Furthermore, the open-circuit and short-circuit resonant states can clearly display the significant differences of the wave patterns between the uncoupled and strongly coupled eigenmodes in the 2D wave systems. Finally, the short-circuit resonant states of the *RLC* network are employed to verify that the experimental Chladni nodal-line patterns in the vibrating plate are the resonant modes subject to the strong coupling between the oscillation system and the driving source.

II. ŠEBA BILLIARDS AND *RLC* CIRCUIT NETWORK WITH A POINT EXCITATION

The original model of the Šeba billiards is a delta potential placed inside a rectangular domain with the Dirichlet boundary condition to study the transition between integrability and chaos in quantum systems. Here we extend the Šeba billiards to consider a general 2D Helmholtz equation for the domain Ω with arbitrary boundary shapes $\delta\Omega$ subject to Dirichlet or

*Corresponding author: Department of Electrophysics, National Chiao Tung University, 1001 Ta-Hsueh Road, Hsinchu 30010, Taiwan; yfchen@cc.nctu.edu.tw

Neumann boundary conditions and a point scatterer in the interior:

$$\left(\frac{\partial^2}{\partial x^2}+\frac{\partial^2}{\partial y^2}+k^2\right)\Psi(x,y;k) = -\alpha\delta(x-x_s)\delta(y-y_s)\Psi(x,y;k), \quad (1)$$

where the parameter α, $\alpha \in (-\infty,\infty)$, is related to the coupling strength of the point scatterer at $(x_s,y_s) \in \Omega$, $\Psi = 0$ on $\delta\Omega$ for the case of the Dirichlet boundary condition, and $\partial\Psi/\partial n = 0$ on $\delta\Omega$ for the case of the Neumann boundary condition. Although the zero-range interaction cannot be rigorously described by using a Dirac δ function in Eq. (1) for 2D billiard problems, it has been verified [3] that Eq. (1) together with a truncated basis can be used to evaluate quantum spectra in 2D billiards with a small but finite-size scatterer. From physical perspectives, the truncation of the basis not only is a consequence of the finiteness of the scatterer size but also practically exists in real systems with the finite potential barrier of the boundary confinement.

For the wave system without the point scatterer, the eigenfunctions ψ_n and eigenvalues λ_n satisfy the equation

$$\left(\frac{\partial^2}{\partial x^2}+\frac{\partial^2}{\partial y^2}+\lambda_n\right)\psi_n(x,y) = 0. \quad (2)$$

The delta function $\delta(x-x_s)\delta(y-y_s)$ and the wave function $\Psi(x,y)$ in Eq. (1) can be approximately expanded with a truncated unperturbed basis $\{\psi_n\}$ $(n = 1,2,3,\ldots,N)$ as

$$\delta(x-x_s)\delta(y-y_s) = \sum_{n=1}^{N}\psi_n^*(x_s,y_s)\psi_n(x,y), \quad (3)$$

$$\Psi(x,y;k) = \sum_{n=1}^{N} c_n(k)\psi_n(x,y). \quad (4)$$

Substituting Eqs. (2)–(4) into Eq. (1), the coefficient $c_n(k)$ can be solved to result in

$$\Psi(x,y;k) = -\alpha\Psi(x_s,y_s)\left[\sum_{n=1}^{N}\frac{\psi_n^*(x_s,y_s)}{k^2-\lambda_n}\psi_n(x,y)\right]. \quad (5)$$

Equation (5) represents that the eigenfunctions of the wave system with the point scatterer are the Green's functions of the free wave system. Nevertheless, the eigenvalues k^2 can be utterly different from the eigenvalues λ_n of the free system. By setting $x = x_s$ and $y = y_s$ in both sides of Eq. (5), the determination of the spectrum k^2 is given by a transcendental equation

$$1+\alpha\,\Xi(x_s,y_s;k) = 0, \quad (6)$$

where

$$\Xi(x_s,y_s;k) = \sum_{n=1}^{N}\frac{|\psi_n(x_s,y_s)|^2}{k^2-\lambda_n}. \quad (7)$$

Here it might be appropriate to call $\Xi(x_s,y_s;k)$ the meromorphic function of 2D singular billiards with a truncated basis. For the limit $\alpha \to \infty$ in the strong-coupling regime, the eigenvalue spectrum $\{k_m\}$ is directly determined by $\Xi(x_s,y_s,k)|_{k=k_m} = 0$. On the other hand, the eigenvalues k^2 for the case $\alpha = 0$ are λ_n, which leads to $\Xi(x_s,y_s;k) \to \infty$.

It has been discussed [2,3] that the Hamiltonian with a Dirac δ function potential in Eq. (1) loses its meaning in the limit of $N \to \infty$ for a complete basis. Under this circumstance, the renormalization process from the self-adjoint extension theory has been used to treat short-range singularities in a proper manner and the eigenvalues are determined by the transcendental equation [1–3]

$$1+\alpha_b\xi(x_s,y_s;k) = 0, \quad (8)$$

where

$$\xi(x_s,y_s;k) = \sum_{n=1}^{\infty}|\psi_n(x_s,y_s)|^2\left(\frac{1}{k^2-\lambda_n}+\frac{\lambda_n}{\lambda_n^2+1}\right). \quad (9)$$

Here α_b is the coupling constant that is formally defined with the formulation based on functional analysis. Since α_b comes from the renormalization process, it does not have a direct relation to physical observables. Nevertheless, it has been fully discussed [3] that α_b can be related to the physical coupling constant α defined in Eq. (1) with a truncated basis. Next, it is verified that the *RLC* circuit network can be exploited to manifest the evolution of eigenstates from closed quantum billiards to the singular billiards with a truncated basis in the strongly coupled limit.

Figure 1(a) shows the schematic configuration of the *RLC* circuit network [14,15]. Each grid point inside the network is connected to its surrounding sites with an inductance L

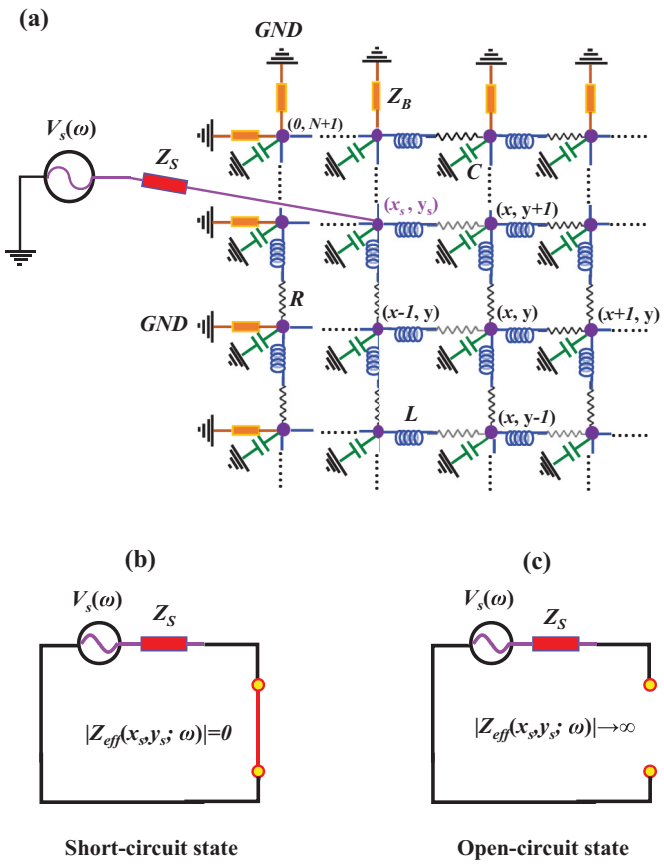

FIG. 1. (Color online) (a) Schematic configuration of the driven *RLC* circuit network. (b) Equivalent short-circuit state. (c) Equivalent open-circuit state.

in series with a resistance R and connected to the ground with a capacitor C. For a small damping, the values of R, L, and C are chosen to satisfy $\sqrt{L/C} \gg R$. The indices (x,y) are used to specify the location of the grid point, where x and y are the horizontal and vertical positions, respectively. A sinusoidal driving source with amplitude V_s and frequency ω is inputted at the grid point specified (x_s,y_s) via a source impedance Z_S to probe the frequency response of the *RLC* network. As shown later, the source impedance Z_S is related to the coupling strength. With Kirchhoff's current law, the voltage at the grid point (x,y) and its surrounding sites satisfies the following difference equation:

$$\frac{[\Phi(x,y+1)+\Phi(x,y-1)+\Phi(x+1,y)+\Phi(x-1,y)-4\Phi(x,y)]}{Z_L}-\frac{\Phi(x,y)}{Z_C}=\frac{[\Phi(x_s,y_s)-V_s]}{Z_S}\delta(x,x_s)\delta(y,y_s), \tag{10}$$

where $Z_L = R + i\omega L$, $Z_C = 1/i\omega C$, and $\delta(x,x_s)$ and $\delta(y,y_s)$ denote the Kronecker delta for a discrete system. Without the source term, Eq. (10) can be reduced to the discrete Helmholtz equation:

$$[\Phi(x,y+1)+\Phi(x,y-1)+\Phi(x+1,y)+\Phi(x-1,y) -4\Phi(x,y)]-\left(\frac{Z_L}{Z_C}\right)\Phi(x,y)=0. \tag{11}$$

The mathematical form of Eq. (11) is equivalent to the Schrödinger equation for billiards problems under the five-point approximation [16]:

$$[\phi_n(x,y+1)+\phi_n(x,y-1)+\phi_n(x+1,y)+\phi_n(x-1,y) - 4\phi_n(x,y)]+\varepsilon_n\phi_n(x,y)=0, \tag{12}$$

where $\phi_n(x,y)$ and ε_n are the eigenvalues and eigenfunctions, respectively.

In terms of the complete set of normalized eigenfunctions $\phi_n(x,y)$, the Kronecker delta function is given by

$$\delta(x,x_s)\delta(y,y_s)=\sum_n \phi_n^*(x_s,y_s)\phi_n(x,y). \tag{13}$$

With the method of self-consistent eigenfunction expansion, the response voltage function Ψ in Eq. (10) can be analytically solved by setting

$$\Phi(x,y;\omega)=\sum_n a_n(\omega)\phi_n(x,y), \tag{14}$$

where the driving frequency ω is included in the argument of the response voltage function in Eq. (14) for a clearer presentation. Substituting Eqs. (12)–(14) into Eq. (10), the coefficient $a_n(\omega)$ can be derived to express the response voltage function as

$$\Phi(x,y;\omega)=\alpha_p[\Phi(x_s,y_s;\omega)-V_s]\left[\sum_n \frac{\phi_n^*(x_s,y_s)\phi_n(x,y)}{(\tilde{\omega}^2-i\tilde{\omega}\gamma-\varepsilon_n)}\right], \tag{15}$$

where $\tilde{\omega}=\omega/\omega_o$, $\omega_o=1/\sqrt{LC}$, $\gamma=R\sqrt{C/L}$, and $\alpha_p = Z_L/Z_S$. The explicit form of the response voltage function $\Phi(x,y;\omega)$ can be obtained by setting $x=x_s$ and $y=y_s$ in both sides of Eq. (15) to find the self-consistent result for the response voltage at the excitation position, $\Phi(x_s,y_s;\omega)$. After some algebra, $\Phi(x_s,y_s;\omega)$ can be in terms of a simple voltage divider equation:

$$\Phi(x_s,y_s;\omega)=\frac{Z_{\rm eff}(x_s,y_s;\omega)}{Z_s+Z_{\rm eff}(x_s,y_s;\omega)}V_s, \tag{16}$$

where $Z_{\rm eff}(x_s,y_s;\omega)$ is the effective impedance of the *RLC* network given by

$$Z_{\rm eff}(x_s,y_s;\omega)=Z_L\left[\sum_n \frac{|\phi_n(x_s,y_s)|^2}{(\varepsilon_n-\tilde{\omega}^2+i\tilde{\omega}\gamma)}\right]. \tag{17}$$

In the denominator in the right-hand side of Eq. (16), the total impedance of the series combination of Z_s and $Z_{\rm eff}(x_s,y_s;\omega)$ can be defined as

$$Z_{\rm tot}(x_s,y_s,\alpha_p;\omega)=Z_s\left[1+\alpha_p\sum_n \frac{|\phi_n(x_s,y_s)|^2}{(\varepsilon_n-\tilde{\omega}^2+i\tilde{\omega}\gamma)}\right]. \tag{18}$$

It can be found that the expression for $Z_{\rm eff}(x_s,y_s;\omega)$ in Eq. (17) with $\gamma=0$ is identical to that of Eq. (7) for the singular billiards via the replacement of $\phi_n(x_s,y_s)\to\psi_n(x_s,y_s)$, $\varepsilon_n\to\lambda_n$, and $\tilde{\omega}^2\to k^2$. There are two sets of resonant frequencies that correspond to $|Z_{\rm eff}(x_s,y_s;\omega)|=0$ and $|Z_{\rm eff}(x_s,y_s;\omega)|\to\infty$, respectively. The resonant frequencies $\{\omega_m\}$ for $|Z_{\rm eff}(x_s,y_s;\omega_m)|=0$ indicate that the *RLC* network behaves as a short-circuit state, as shown in Fig. 1(b), equivalent to the eigenvalue spectrum $\{k_m\}$ of the singular billiards in the strong-coupling regime. On the other hand, when the driving frequency $\tilde{\omega}$ is equal to any eigenvalue ε_n and $|\phi_n(x_s,y_s)|\neq 0$, the *RLC* network behaves as an open-circuit state with $|Z_{\rm eff}(x_s,y_s;\omega_o\varepsilon_n)|\to\infty$, as shown in Fig. 1(c). In other words, the open-circuit and short-circuit resonant modes represent the network to be in the uncoupled and strongly coupled states, respectively. Note that the condition $|\phi_n(x_s,y_s)|=0$ means the position of the driving source is just at the nodal point of the eigenmode $\phi_n(x,y)$ of the free *RLC* network. Under the circumstance of $|\phi_n(x_s,y_s)|=0$, the resonant frequencies $\omega_o\varepsilon_n$ for the open-circuit states will disappear in the impedance spectrum. To be brief, the resonant spectrum $|Z_{\rm eff}(x_s,y_s;\omega_m)|=0$ can be used to mimic the eigenvalue spectrum $\{\omega_m\}$ of the Šeba billiards and the resonant spectrum $|Z_{\rm eff}(x_s,y_s;\omega_o\varepsilon_n)|\to\infty$ can manifest the eigenvalues $\{\varepsilon_n\}$ of the free billiards as long as $|\phi_n(x_s,y_s)|\neq 0$. It is not only physically intriguing but also pedagogically meaningful that the nearly uncoupled and extremely strongly coupled eigenstates in the wave systems can be elucidated with the equivalent open-circuit and short-circuit resonant states of the *RLC* network, respectively.

Substituting Eqs. (16) and (17) into Eq. (15) can lead the response voltage function to be given by

$$\Phi(x,y;\omega) = \frac{V_s Z_L}{Z_S + Z_{\rm eff}(x_s,y_s;\omega)} \left[\sum_n \frac{\phi_n^*(x_s,y_s)\phi_n(x,y)}{(\varepsilon_n - \tilde{\omega}^2 + i\tilde{\omega}\gamma)} \right]. \tag{19}$$

Analogous to Eq. (5) for the singular billiards, the response voltage functions $\Phi(x,y;\omega)$ in Eq. (19) are the Green's functions of the *RLC* network system. At the resonant frequencies $\{\omega_m\}$ for the short-circuit states $|Z_{\rm eff}(x_s,y_s;\omega_m)| = 0$, the response functions $\Phi(x,y;\omega_m)$ can be employed to emulate the eigenfunctions $\Psi(x,y;k_m)$ of the singular billiards in the limit $\alpha \to \infty$ of the strong-coupling regime. On the other hand, at the resonant frequencies $\{\omega_o\varepsilon_n\}$ for the open-circuit states $|Z_{\rm eff}(x_s,y_s;\omega_o\varepsilon_n)| \to \infty$, the response functions $\Phi(x,y;\omega_o\varepsilon_n)$ can imitate the eigenfunctions $\{\phi_n(x,y)\}$ of the free billiards. It is worthwhile mentioning that only the open-circuit resonant states of the *RLC* network have been proposed to emulate the eigenfunctions of the quantum billiards [14–16], whereas the short-circuit resonant states have not been exploited to explore the systems with strong coupling.

III. NUMERICAL RESULTS AND DISCUSSION

A square-shaped *RLC* network with $N \times N$ internal grids is exploited to manifest the present analysis. The eigenfunctions and eigenvalues of the square-shaped *RLC* network can be exactly solved by employing the theory of linear chain coupled oscillators as [17]

$$\phi_{n_1,n_2}(x,y) = \frac{2}{N+1} \sin\left(\frac{n_1\pi}{N+1}x\right) \sin\left(\frac{n_2\pi}{N+1}y\right), \tag{20}$$

and

$$\varepsilon_{n_1,n_2} = 4\left\{ \sin^2\left[\frac{n_1\pi}{2(N+1)}\right] + \sin^2\left[\frac{n_2\pi}{2(N+1)}\right] \right\}, \tag{21}$$

where $n_1 = 1,2,\ldots,N$, $n_2 = 1,2,\ldots,N$, and the location indices x and y are integers running from 0 to $N+1$. Note that 0 and $N+1$ are the lowest and highest indices to denote the sites at the boundary. Due to the separable property, the eigenfunctions $\phi_{n_1,n_2}(x,y)$ are specified with two quantum numbers, n_1 and n_2. Therefore, the effective impedance in Eq. (17) for the square *RLC* network can be explicitly written as

$$Z_{\rm eff}(x_s,y_s;\omega) = Z_L \sum_{n_2=1}^{N} \sum_{n_1=1}^{N} \frac{|\phi_{n_1,n_2}(x_s,y_s)|^2}{(\varepsilon_{n_1,n_2} - \tilde{\omega}^2 + i\tilde{\omega}\gamma)}. \tag{22}$$

Similarly, the response function $\Phi(x,y;\omega)$ for the square *RLC* network is given by

$$\Phi(x,y;\omega) = \frac{V_s Z_L}{Z_S + Z_{\rm eff}(x_s,y_s;\omega)} \times \left[\sum_{n_2=1}^{N} \sum_{n_1=1}^{N} \frac{\phi_{n_1,n_2}^*(x_s,y_s)\phi_{n_1,n_2}(x,y)}{(\varepsilon_{n_1,n_2} - \tilde{\omega}^2 + i\tilde{\omega}\gamma)} \right]. \tag{23}$$

The parameters used in the calculation are as follows: $V_s = 10$ V, $L = 10$ mH, $C = 10$ mF, $R = 0.05$ mΩ, $Z_S = 1$ Ω, and $N = 301$. Hereafter the values of the parameters are used throughout this paper unless otherwise specified.

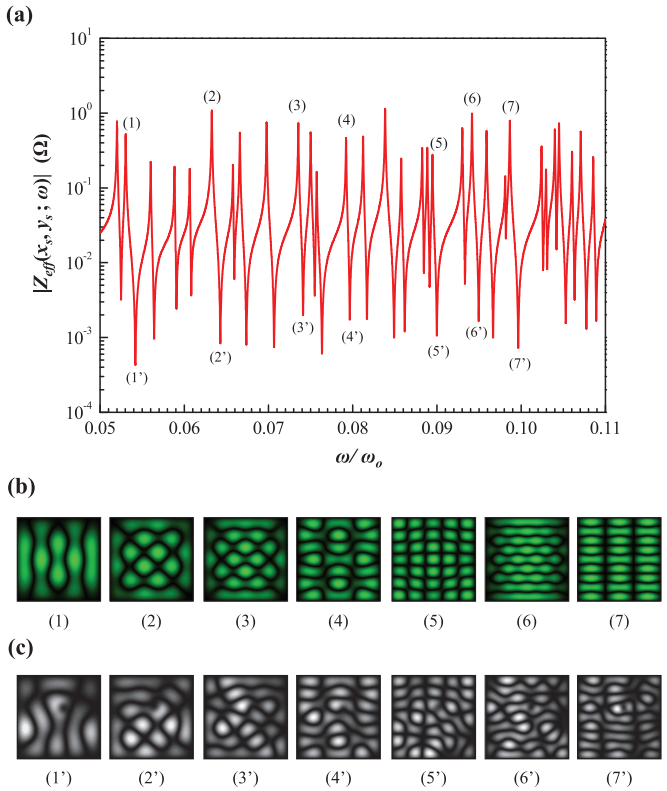

FIG. 2. (Color online) (a) Calculated results of the effective impedance $|Z_{\rm eff}(x_s,y_s;\omega)|$ in Eq. (23) as a function of the driving frequency ω for the case of $(x_s,y_s) = (163,183)$. (b) Numerical open-circuit patterns $|\Phi(x,y;\omega)|^2$ at the resonance frequencies $\tilde{\omega} = \varepsilon_{n_1,n_2}$ marked by (1)–(7) in (a). (c) Numerical short-circuit patterns $|\Phi(x,y;\omega)|^2$ at the resonance frequencies $\omega = \omega_m$ marked by (1′)–(7′) in (a).

As discussed earlier, the location of the driving source can affect the occurrence of the resonant states, depending on $|\phi_{n_1,n_2}(x_s,y_s)| = 0$ or $|\phi_{n_1,n_2}(x_s,y_s)| \neq 0$. To demonstrate the influence of the location of the driving source, two different positions $(x_s,y_s) = (151,151)$ and $(x_s,y_s) = (163,183)$ are used in the simulation, respectively. Note that $(x_s,y_s) = (151,151)$ is just at the center of the network; i.e., $x_s = (N+1)/2$ and $y_s = (N+1)/2$.

Figure 2(a) shows the calculated results of the effective impedance $|Z_{\rm eff}(x_s,y_s;\omega)|$ in Eq. (22) as a function of the driving frequency ω for the case of $(x_s,y_s) = (163,183)$. It can be seen that the spectrum of the effective impedance displays numerous sharp peaks and dips that represent the open-circuit and short-circuit resonant states, respectively. Figure 2(b) depicts several open-circuit patterns $|\Phi(x,y;\omega)|^2$ for the response function at the resonance frequencies $\tilde{\omega} = \varepsilon_{n_1,n_2}$ marked by (1)–(7) in Fig. 2(a). The wave patterns of the open-circuit states can be seen to exhibit features symmetrical to those of eigenmodes of the square billiards. Figure 2(c) shows several short-circuit patterns $|\Phi(x,y;\omega)|^2$ for the response function at the resonance frequencies $\omega = \omega_m$ marked by (1′)–(7′) in Fig. 2(a). The short-circuit states can be found to reveal the irregular interference patterns that mainly come from the superposition of several eigenmodes with eigenvalues ε_{n_1,n_2} in the neighborhood of the resonance

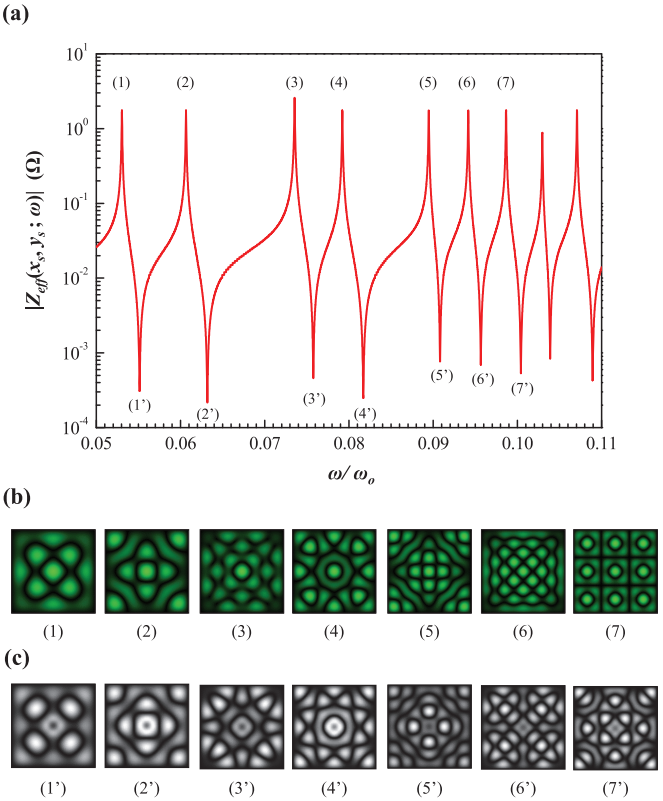

FIG. 3. (Color online) (a) Calculated results of the effective impedance $|Z_{\text{eff}}(x_s,y_s;\omega)|$ in Eq. (23) as a function of the driving frequency ω for the case of $(x_s,y_s)=(151,151)$. (b) Numerical open-circuit patterns $|\Phi(x,y;\omega)|^2$ at the resonance frequencies $\tilde{\omega}=\varepsilon_{n_1,n_2}$ marked by (1)–(7) in (a). (c) Numerical short-circuit patterns $|\Phi(x,y;\omega)|^2$ at the resonance frequencies $\omega=\omega_m$ marked by (1′)–(7′) in (a).

frequencies $\tilde{\omega}=\omega_m/\omega_o$. The relative contributions of the superposed eigenmodes in the short-circuit resonant state can be precisely computed with Eq. (23).

Figure 3 shows the results for the case of $(x_s,y_s)=(151,151)$ with plots similar to those shown in Fig. 2. The number of the resonance frequencies in Fig. 3(a) can be clearly seen to be considerably less than that in Fig. 2(a). As shown in Eq. (22), the missing eigenfrequencies comes from the central driving source $(x_s,y_s)=(151,151)$ to lead to $|\phi_{n_1,n_2}(x_s,y_s)|=0$ for any even index of n_1 or n_2. In contrast, the source position at $(x_s,y_s)=(163,183)$ for the results shown in Fig. 2 belongs to an asymmetric location and the condition $|\phi_{n_1,n_2}(x_s,y_s)|=0$ never occurs for all eigenfunctions of the free system. As seen from Eq. (17) for the effective impedance, the location of the source determines the weighting factor $|\phi_{n_1,n_2}(x_s,y_s)|^2$ for each eigenmode with eigenvalue ε_{n_1,n_2} and affects the appearance of the eigenfunctions. Therefore, the selection of the location of the source is important for using the *RLC* circuit network to imitate the eigenfunctions of the billiard system. Numerous different locations for the source generally need to be individually employed to excite all the eigenfunctions. On the other hand, the precision of the imitation for the eigenfunctions can be essentially enhanced by increasing of the grid number N.

IV. APPLICATIONS TO CHLADNI RESONANT PATTERNS

The Chladni plate experiment is one of the most historical and classical 2D resonant wave systems, which acts as a precursor for various resonance problems. Chladni nodal-line patterns are formed by the sand particles that stop at the nodes of the resonant modes on a vibrating plate. Currently, the Chladni experiment is performed by using an electronically controlled mechanical oscillator to locally drive the plate with variable frequency. In the monumental work of acoustics, Rayleigh proposed the construction of sound figures by the Helmholtz equation instead of the biharmonic equation [18,19] to greatly reduce the mathematical complexity. Nevertheless, since the strong coupling between the oscillation system and the driving source [20–23] leads to the resonant spectrum being utterly different from the eigenvalue spectrum of the homogeneous equation, the eigenfunctions of the Helmholtz equation cannot directly correspond to the experimental patterns [20,24]. Here we exploit the short-circuit resonant states of the *RLC* network to confirm that the experimental nodal-line patterns in the vibrating plate are the resonant modes subject to the strong coupling between the oscillation system and the driving source.

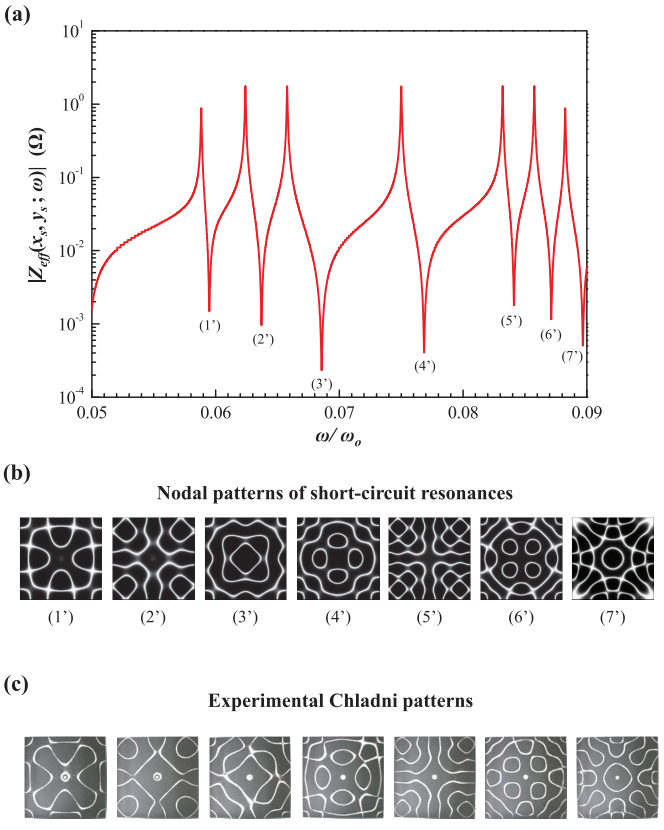

FIG. 4. (Color online) (a) Calculated results of the effective impedance as a function of the driving frequency for the excitation source at the central position of $(x_s,y_s)=(151,151)$ for the square *RLC* network with the Neumann boundary condition. (b) Nodal-line patterns for the short-circuit resonant states marked by (1′)–(7′) in (a). (c) Experimental nodal-line patterns obtained in the Chladni experiment with the same excitation condition and the same mode orders are shown in (c).

Since the boundary condition of the vibrating plate is the Neumann type, the eigenfunctions of the square *RLC* network in Eq. (20) are changed as

$$\phi_{n_1,n_2}(x,y) = \frac{2}{N+1}\cos\left(\frac{n_1\pi}{N+1}x\right)\cos\left(\frac{n_2\pi}{N+1}y\right), \quad (24)$$

where $n_1 = 0,1,2,\ldots,N, n_2 = 0,1,2,\ldots,N$, and the location indices x and y are integers running from 0 to $N+1$. The parameters used in the calculation are as follows: $V_s = 10\,\mathrm{V}$, $L = 10$ mH, $C = 10$ mF, $R = 0.05$ mΩ, $Z_S = 1$ Ω, and $N = 301$. Figure 4(a) shows calculated results of the effective impedance as a function of the driving frequency for the excitation source at the central position of $(x_s, y_s) = (151,151)$ for the square *RLC* network with the Neumann boundary condition. Figure 4(b) depicts several nodal-line patterns for the short-circuit resonant states marked by (1′)–(7′) in Fig. 4(a). Note that the numerical nodal-line patterns are plotted by the inverse of the wave patterns, $|\Phi(x,y;\ \omega_m)|^2$. The experimental nodal-line patterns obtained in the Chladni experiment with the same excitation condition and the same mode orders are shown in Fig. 4(c) for comparison. The details of the experiment can be found in Ref. [20]. It can be seen that the nodal-line patterns of the short-circuit states are in good agreement with the experimental results of the resonant Chladni modes. In addition, Fig. 5 depicts the same plots as shown in Fig. 4 for the excitation source at the off-center position of $(x_s, y_s) = (163,183)$. The overall nodal-line structures of the short-circuit states are rather similar to those of the resonant modes in the Chladni experiment. The good similarity confirms that the resonant modes related to the Chladni patterns come from the vibrating plate subject to the strong coupling with the exciter.

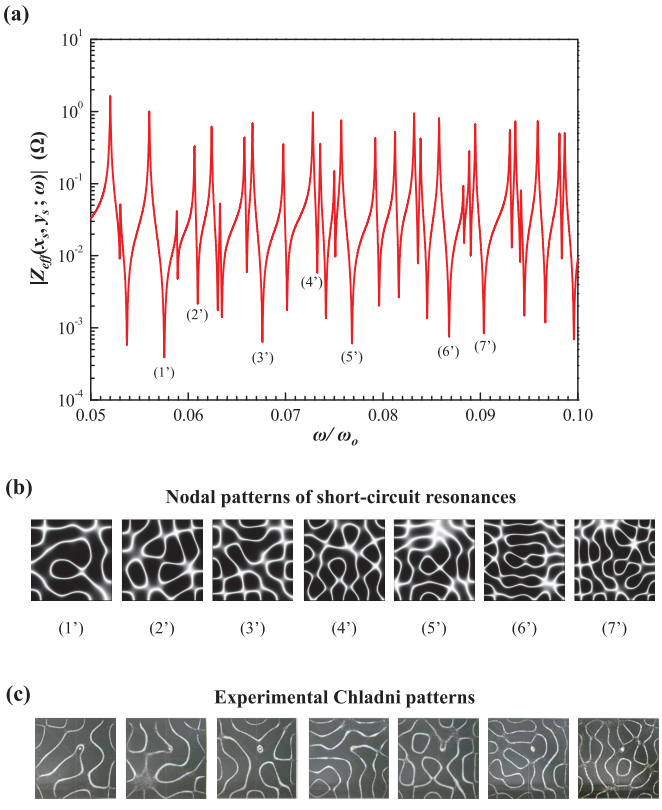

FIG. 5. (Color online) (a) Calculated results of the effective impedance as a function of the driving frequency for the excitation source at the asymmetric position of $(x_s, y_s) = (163,183)$ for the square *RLC* network with the Neumann boundary condition. (b) Nodal-line patterns for the short-circuit resonant states marked by (1′)–(7′) in (a). (c) Experimental nodal-line patterns obtained in the Chladni experiment with the same excitation condition and the same mode orders are shown in (c).

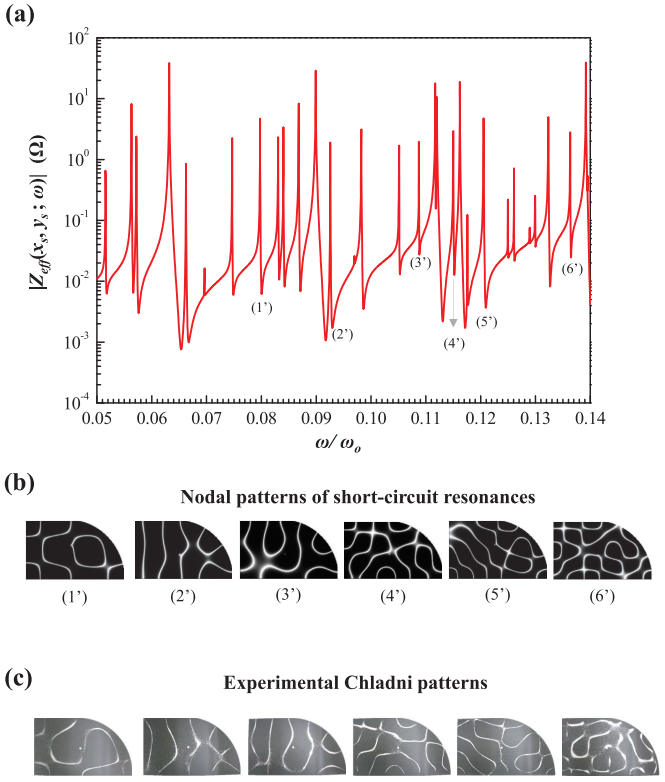

FIG. 6. (Color online) (a) Calculated results of the effective impedance as a function of the driving frequency for the excitation source at the position of $(x_s, y_s) = (92,66)$ for the quarter-stadium-shaped *RLC* network with the Neumann boundary condition. (b) Nodal-line patterns for the short-circuit resonant states marked by (1′)–(6′) in (a). (c) Experimental nodal-line patterns obtained in the Chladni experiment with the same excitation condition and the same mode orders are shown in (c).

To further explore the practicability, the commercial HSPICE software was exploited to program the *RLC* circuit networks with arbitrary shapes. A quarter-stadium-shaped network with 200×114 grids along the horizontal and vertical axes was considered. The parameters of the electric components in the simulation are the same as those used in the square-shaped network. Figure 6(a) shows the effective impedance as a function of the driving frequency for the excitation source at the position of $(x_s, y_s) = (92,66)$. Figure 6(b) plots several nodal-line patterns for the short-circuit resonant states marked by (1′)–(6′) in Fig. 6(a). For comparison, a quarter-stadium-shaped plate was fabricated to obtain the experimental nodal-line Chladni patterns with the same excitation condition. Figure 6(c) depicts the experimental results with the mode orders close to those shown in Fig. 6(b). Once again, the experimental results of the resonant Chladni modes agree very

well with the nodal-line patterns of the short-circuit states. In other words, the Chladni resonant patterns can be related to the eigenfunctions of the singular billiards for regular as well as chaotic shapes.

V. CONCLUSIONS

In summary, the coupling interaction between the driving source and the *RLC* network has been explored by deriving the effective impedance. The mathematical form of the derived effective impedance has been verified to be identical to the meromorphic function of the singular billiards with a truncated basis. The frequency spectrum of the derived impedance function clearly displays the open-circuit and short-circuit resonant states that have been shown to correspond to the eigenstates of closed quantum billiards and the singular billiards in the strongly coupled limit, respectively. With the response voltage function of the *RLC* network, the significant difference of the wave patterns between the uncoupled and strongly coupled eigenmodes in the 2D wave systems has been clearly demonstrated. Finally, the short-circuit resonant states are employed to make a comparison with the experimental Chladni nodal-line patterns in the vibrating plate. The good agreement confirms that the Chladni patterns are the resonant modes subject to the strong coupling between the oscillation system and the driving source.

ACKNOWLEDGMENTS

This work is supported by the Ministry of Science and Technology of Taiwan (Contract No. MOST-103-2112-M-009-016-MY3).

[1] P. Šeba, Wave Chaos in Singular Quantum Billiard, Phys. Rev. Lett. **64**, 1855 (1990).
[2] T. Shigehara, Conditions for the appearance of wave chaos in quantum singular systems with a pointlike scatterer, Phys. Rev. E **50**, 4357 (1994).
[3] T. Shigehara and T. Cheon, Wave chaos in quantum billiards with a small but finite-size scatterer, Phys. Rev. E **54**, 1321 (1996).
[4] E. Bogomolny, U. Gerland, and C. Schmit, Singular statistics, Phys. Rev. E **63**, 036206 (2001).
[5] G. Berkolaiko, J. P. Keating, and B. Winn, Intermediate Wave Function Statistics, Phys. Rev. Lett. **91**, 134103 (2003).
[6] T. Tudorovskiy, U. Kuhl, and H.-J. Stöckmann, Singular statistics revised, New J. Phys. **12**, 123021 (2010).
[7] Z. Rudnick and H. Ueberschär, Statistics of wave functions for a point scatterer on the torus, Commun. Math. Phys. **316**, 763 (2012).
[8] H. Ueberschär, Quantum chaos for point scatterers on flat tori, Philos. Trans. R. Soc., A **372**, 20120509 (2014).
[9] C. Gough, The violin: Chladni patterns, plates, shells and sounds, Eur. Phys. J: Spec. Top. **145**, 77 (2007).
[10] L. Novotny, Strong coupling, energy splitting, and level crossings: A classical perspective, Am. J. Phys. **78**, 1199 (2010).
[11] M. L. Zimmerman, M. G. Littman, M. M. Kash, and D. Kleppner, Stark structure of the Rydberg states of alkali-metal atoms, Phys. Rev. A **20**, 2251 (1979).
[12] M. Bayer, P. Hawrylak, K. Hinzer, S. Fafard, M. Korkusinski, Z. R. Wasilewski, O. Stern, and A. Forchel, Coupling and entangling of quantum dot states in quantum dot molecules, Science **291**, 451 (2001).
[13] T. J. Kippenberg and K. J. Vahala, Cavity optomechanics: Back-action at the mesoscale, Science **321**, 1172 (2008).
[14] E. N. Bulgakov, D. N. Maksimov, and A. F. Sadreev, Electric circuit networks equivalent to chaotic quantum billiards, Phys. Rev. E **71**, 046205 (2005).
[15] O. Bengtsson, J. Larsson, and K.-F. Berggren, Emulation of quantum mechanical billiards by electrical resonance circuits, Phys. Rev. E **71**, 056206 (2005).
[16] K.-F. Berggren, J. Larsson, and O. Bengtsson, Electrical resonance circuits as analogs to quantum mechanical billiards, Acta Phys. Pol., A **109**, 33 (2006).
[17] W. Greiner, *Classical Mechanics: Systems of Particles and Hamiltonian Dynamics*, 2nd ed. (Springer, New York, 2010).
[18] T. Wah, Vibration of circular plates, J. Acoust. Soc. Am. **34**, 275 (1962).
[19] Lord Rayleigh, *Theory of Sound* (Dover, New York, 1945), pp. 363–381.
[20] P. H. Tuan, C. P. Wen, P. Y. Chiang, Y. T. Yu, H. C. Liang, K. F. Huang, and Y. F. Chen, Exploring the resonant vibration of thin plates: Reconstruction of Chladni patterns and determination of resonant wave numbers, J. Acoust. Soc. Am. **137**, 2113 (2015).
[21] I. V. Zozoulenko and K.-F. Berggren, Quantum scattering, resonant states, and conductance fluctuations in an open square electron billiard, Phys. Rev. B **56**, 6931 (1997).
[22] K. Schaadt, A. P. B. Tufaile, and C. Ellegaard, Chaotic sound waves in a regular billiard, Phys. Rev. E **67**, 026213 (2003).
[23] M. D. Waller, Vibration of free circular plates. Part 2: Compounded normal modes, Proc. Phys. Soc. **50**, 77 (1938).
[24] M. D. Waller, Vibration of free square plates: Part II, compounded normal modes, Proc. Phys. Soc. **52**, 452 (1940).